Harmonization with Flow-based Causal Inference

Rongguang Wang[1,2], Pratik Chaudhari[1,3], and Christos Davatzikos[1,2,4]

[1] Department of Electrical and Systems Engineering, University of Pennsylvania
[2] Center for Biomedical Image Computing and Analytics (CBICA)
[3] General Robotics, Automation, Sensing and Perception Laboratory (GRASP)
[4] Department of Radiology, Perelman School of Medicine, University of Pennsylvania
{rgw@seas, pratikac@seas, Christos.Davatzikos@pennmedicine}.upenn.edu

Abstract. Heterogeneity in medical data, e.g., from data collected at different sites and with different protocols in a clinical study, is a fundamental hurdle for accurate prediction using machine learning models, as such models often fail to generalize well. This paper presents a normalizing-flow-based method to perform counterfactual inference upon a structural causal model (SCM) to harmonize such data. We formulate a causal model for observed effects (brain magnetic resonance imaging data) that result from known confounders (site, gender and age) and exogenous noise variables. Our method exploits the bijection induced by flow for harmonization. We can infer the posterior of exogenous variables, intervene on observations, and draw samples from the resultant SCM to obtain counterfactuals. We evaluate on multiple, large, real-world medical datasets to observe that this method leads to better cross-domain generalization compared to state-of-the-art algorithms. Further experiments that evaluate the quality of confounder-independent data generated by our model using regression and classification tasks are provided.

Keywords: Harmonization · Causal inference · Normalizing flows

1 Introduction

Deep learning models have shown great promise in medical imaging diagnostics [11] and predictive modeling with applications ranging from segmentation tasks [19] to more complex decision-support functions for phenotyping brain diseases and personalized prognosis. However deep learning models tend to have poor reproducibility across hospitals, scanners, and patient cohorts; these high-dimensional models tend to overfit to specific datasets and generalize poorly across training data [6]. One potential solution to the above problem is to train on very large and diverse databases but this can be prohibitive, because data may change frequently (e.g., new imaging devices are introduced) and gathering training labels for medical images is expensive. More importantly, even if it were possible to train a model on data that covers all possible variations across images, such a model would almost certainly sacrifice accuracy in favor of

generalization—it would rely on coarse imaging features that are stable across, say imaging devices and patient populations, and might fail to capture more subtle and informative detail. We need new methods that can tackle heterogeneity in medical data without sacrificing predictive accuracy. We would like to develop methods for "data harmonization", for instance, they would allow training a classifier on, say data from one site, and obtaining similar predictive accuracy on data from another site.

Contributions We model brain imaging data and clinical variables using a causal graph and focus on how causes (site, gender and age) result in the effects, namely imaging measurements (herein we use region of interest (ROI) volumes obtained by preprocessing brain MRI data). We show how to use a normalizing flow parameterized using deep networks to learn the structural assignments in this causal graph. We demonstrate how harmonization of data can be performed efficiently using efficient counterfactual inference on this flow-based causal model. Essentially, we answer the counterfactual question "what would the scans look like if they had been acquired from the same site". For example, given a dataset pertaining to one site (source), we perform a counterfactual query to synthesize the dataset, as if it were from another site (target). We demonstrate results of such harmonization on regression (age prediction) and classification (predicting Alzheimer's disease) tasks using several large-scale brain imaging datasets. We demonstrate substantial improvement over competitive baselines on these tasks.

2   Related Work

To remove the undesired counfoundings, especially sites or scanners, from imaging data, a wide range of contributions has been made by employing the recent advances in statistical and machine learning [16,29,21,22,31,3]. Based on parametric empirical bayes [20], ComBat methods [16,29] produce site-removed image features by performing location (mean) and scale (variance) adjustments to the data. The linear model estimates the location and scale differences in images features cross-site, while preserving other confounders such as sex and age. Since ComBat [16,29] only considered covariates sex and age in modelling, other unknown variations such as race and disease are removed together with the site variable, which might leads to unsatisfactory performance in downstream tasks, e.g. disease diagnosis. On the other hand, generative deep learning models such as variational autoencoders (VAEs) [18] and generative adversarial networks (GANs) [12] have been used in many works [21,22,31,3]. In order to disentangle the scanner-specific information from the images, [21,22] propose to minimize the mutual information between the site variable and image embedding in the latent space of a VAE with conditional decoder. Then, the site-invariant representations can be composed with a reference site variable to reconstruct images at the same site. To avoid the blurriness problem of VAEs, unsupervised image-to-image translation has been proposed to map scans either between two sites [31] or to a reference domain [3] using CycleGAN [36]. However, GANs usually suffer from mode collapse and convergence issues, especially for 3D images.

3   Method

3.1   Building blocks

Our method builds upon the causal inference mechanism proposed by Judea Pearl [26]. The first "rung" of this ladder consists of associative queries which are about understanding correlations; they are concerned with conditional probability statements $P(y \mid x)$ of events $Y = y$ given observations $X = x$. The second, called intervention, asks questions like "what happens if we do ...". This requires structural assumptions based on prior knowledge about the underlying data generation model and is formalized using Pearl's do-calculus as $P(y \mid \mathrm{do}(\tilde{x}))$ which denotes the probability of $Y = y$ given that we intervene and set $X = \tilde{x}$. Counterfactuals address retrospective queries, e.g., "would $Y = \tilde{y}$ happen if we $\mathrm{do}(\tilde{x})$ given that $Y = y$ happened when $X = x$". This is written as the probability $P(\tilde{y}_{\tilde{x}} \mid y, x)$. Counterfactual queries are at the top of the causal inference hierarchy because they subsume associational and interventional queries.

Structural Causal Models (SCMs) are analogues of directed probabilistic graphical models for causal inference [28,32]. Roughly speaking, parent-child relationships in an SCM denote the effect (child) of direct causes (parents) while they only denote conditional independencies in a graphical model. Consider a collection of random variables $x = (x_1, \ldots, x_m)$, an SCM given by $M = (S, P_\epsilon)$ consists of a collection $S = (f_1, \ldots, f_m)$ of assignments $x_k = f_k(\epsilon_k; \mathrm{pa}_k)$ where pa_k denotes the set of parents (direct causes) of x_k and noise variables ϵ_k are unknown and unmodeled sources of variation for x_k. Each variable x_k is independent of its non-effects given its direct causes (known as the causal Markov condition), we can write the joint distribution of an SCM as $P_M(x) = \prod_{k=1}^{m} P(x_k \mid \mathrm{pa}_k)$; each conditional distribution here is determined by the corresponding structural assignment f_k and noise distribution [26]. Exogenous noise variables are assumed to have a joint distribution $P_\epsilon = \prod_{k=1}^{m} P(\epsilon_i)$, this will be useful in the sequel.

Counterfactual Inference   Given a SCM, a counterfactual query is formulated as a three-step process, namely, abduction, action, and prediction [26,28,27]. First, we predict exogenous noise ϵ based on observations to get the posterior $P_M(\epsilon \mid x) = \prod_{k=1}^{m} P_M(\epsilon_k \mid x_k, \mathrm{pa}_k)$. Then comes intervention denoted by $\mathrm{do}(\tilde{x}_k)$, where we replace structural assignments of variable x_k. Intervention makes the effect x_k independent of both its causes pa_k and noise ϵ_k and this results in a modified SCM $\tilde{M} = M_{\mathrm{do}(\tilde{x})} \equiv (\tilde{S}, P_M(\epsilon \mid x))$. Note that the noise distribution has also been modified, it is now the posterior $P_M(\epsilon \mid x)$ obtained in the abduction step. The third step, namely prediction involves predicting counterfactuals by sampling from the distribution $P_{\tilde{M}}(x)$ entailed by the modified SCM.

Learning a normalizing flow-based SCM   Given the structure of the SCM, learning the model involves learning the structure assignments S from data. We next discuss how to exploit deep networks to do so using normalizing flows. This
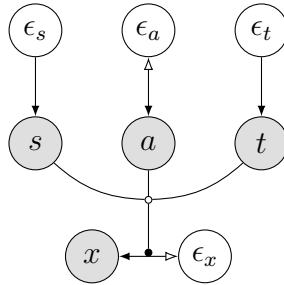
Fig. 1: Causal graph of the structural causal model for brain imaging. The model is constructed with observations, namely brain scans (x), sex (s), age (a), and imaging site (t), and their exogenous variables $(\epsilon_x, \epsilon_s, \epsilon_a,$ and $\epsilon_t)$. The bidirectional arrows indicate invertible normalizing flow models and the black dot shows that the flow model associated with x is conditioned on the direct causes (parents) s, a, and t. To answer the counterfactual question "what would the scans look like if they had been acquired from the same site", we build the model in the order of the causation ladder, namely, association, intervention, and counterfactuals. Firstly, we train the flow-based SCM M_θ with passively observed data (image features x, sex s, age a, and site t) to obtain association ability. Then, we infer the posterior exogenous variables ϵ_x and ϵ_a with the invertible structural assignments (abduction step). Next, by replacing site variable t with a specific value τ, we intervene the structural assignment to the same site $(\mathrm{do}(t = \tau))$. Finally, we sample from the modified flow-based SCM $M_{\mathrm{do}(t=\tau)}$ to obtain counterfactual queries.

will have the additional benefit that we will be able to use normalizing flows to efficiently the abduction and prediction steps above and obtain an efficient method for counterfactual inference. Normalizing flows model a complex probability density as the result of a transformation applied to some simple probability density [23,24,7,10]; these transformations are learned using samples from the target. Formally, given observed variables x and base density $\epsilon \sim p(\epsilon)$, we want to find an invertible and differentiable transformation $x = f(\epsilon)$. The probability density of x is given by $p(x) = p(\epsilon)|\det\nabla f(\epsilon)|^{-1}$ where $\epsilon = f^{-1}(x)$ and $\nabla f(\epsilon)$ is the Jacobian of the "flow" $f : \epsilon \mapsto x$. The density $p(\epsilon)$ can be anything but it is typically chosen to be a Gaussian for convenience. Fitting a θ-parametrized normalizing flow f_θ can done using a maximum-likelihood objective:

$$\theta^* = \operatorname{argmax} \frac{1}{n} \sum_{i=1}^{n} \log p(\epsilon^i) - \log |\det\nabla f_\theta(\epsilon^i)|,$$

on a dataset samples $D = \{x^i \sim p(x)\}_{i=1}^{n}$ with n samples; here $e^i = f_\theta^{-1}(x^i)$. Parameterizing a normalizing flow using a deep network leads to powerful density estimation methods. This approach can be easily extended to conditional densities of the form $p(x_k \mid \mathrm{pa}_k)$ in our SCM.

3.2 Harmonization using counterfactual inference in a flow-based SCM

Given the structure of a SCM, we fit conditional flows $f_{\theta_k} : \epsilon_k \mapsto x_k$ that map exogenous noise to effect x_k given parents pa_k for all nodes in the SCM. Effectively, we are modeling all structural assignment functions using flows. We will denote the combined flow for all nodes in the SCM as f_θ which maps noise $\epsilon^i = (\epsilon_1^i, \ldots, \epsilon_m^i)$ to observations $x^i = (x_1^i, \ldots, x_m^i)$ in the dataset; the corresponding SCM is denoted by M_θ. Focus on a particular datum x^i in the dataset. The abduction step simply computes $\epsilon^i = f_\theta^{-1}(x^i)$. Formally this corresponds to computing the posterior distribution $P_{M_\theta}(\epsilon \mid x^i)$. The next step, namely, intervention uses the fact that the flow models a conditional distribution and replaces (intervenes) the value of a particular variable, say $x_k^i \leftarrow \tilde{x}_k^i$; this corresponds to the operation $\mathrm{do}(\tilde{x}_k)$. The variable x_k is decoupled from its parents and exogenous noise which corresponds to a modified structural assignment $\tilde{f}_{\theta_k}$ and results in a new SCM $\tilde{M}_\theta$. We can now run the same flow $\tilde{f}_\theta$ forwards using samples ϵ^i from the abduction step to get samples from $P_{\tilde{M}_\theta}(x)$ which are the counterfactuals. Fig. 1 shows an example SCM for brain imaging data and shows we perform counterfactual queries to remove site effects.

4 Experimental Results

4.1 Setup

Datasets We use 6,921 3D T1-weighted brain magnetic resonance imaging (MRI) scans acquired from multiple scanners or sites in Alzheimer's Disease Neuroimaging Initiative (ADNI) [15] and iSTAGING consortium [13] which consists of Baltimore Longitudinal Study of Aging (BLSA) [30,2], Study of Health in Pomerania (SHIP) [14], and UK Biobank (UKBB) [33]. The detailed demographic information of the datasets is provided in the Appendix. We first perform a sequence of preprocessing steps on these images, including bias-filed correction [34], brain tissue extraction via skull-stripping [8], and multi-atlas segmentation [9]. Each scan is then segmented into 145 anatomical regions of interests (ROIs) spanning the entire brain, and finally volumes of the ROIs are taken as the features. In the experiments, we perform age prediction task using iSTAGING consortium where the age of participants is range from 21 to 93 years old. We also demonstrate the effectiveness of our method on Alzheimer's disease (AD) classification task which is more challenging than age prediction using ADNI dataset where the diagnosis groups including cognitive normal (CN) and AD.

Implementation We implement three variants of flow-based SCM with different flow types (affine, linear and quadratic autoregressive splines [7,10]) using PyTorch [25] and Pyro [4]. To construct each flow-based SCM, we predict logits for sex and site variables and fit normalizing flows for other structural assignments. Specifically, a linear flow and a conditional flow (conditioned on activations of a fully-connected network that takes age, sex and scanner ID as input) are used as
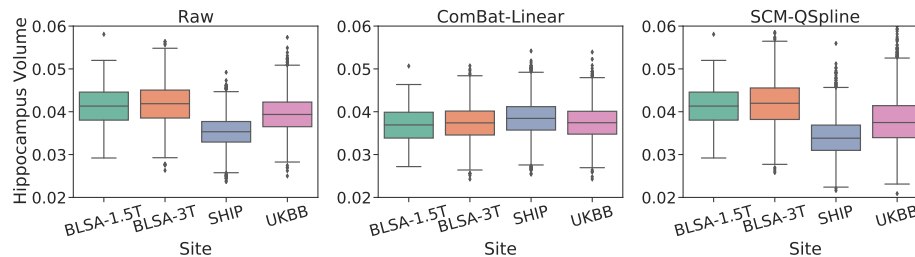
Fig. 2: Comparison of normalized feature (hippocampus volume) distributions cross-site in iSTAGING consortium before (raw) and after apply ComBat and the proposed method (SCM). We observe that ComBat aligned inter-site feature distributions by preserving sex and age effects and remove all other unknown confounding effects which are treated as site effects. In contrast, the distribution of hippocampus volume is unchanged after applied our proposed method which takes both known confoundings (sex, age, and site) and unknown confoudings (as exogenous noises) into consideration. ComBat removes these useful confounders which is detrimental to accuracy as shown in Table 2.

structural assignments for age and ROI features respectively. Standard Gaussian is used as the density for all exogenous noise. During training, we use Adam [17] with batch-size of 64, initial learning rate 3×10^{-4}, and weight decay 10^{-4} for optimization. We utilize a step-based learning rate schedule with decay milestones at 50% and 75% of the total epochs in training. All models are trained for at most 100 epochs. We report the implementation details of flow-based SCM and classifier, and the best validation log-likelihood for each model in the Appendix.

Baselines To evaluate the performance of our proposed method, we compare with state-of-the-art algorithms: invariant risk minimization (IRM) [1], ComBat [16,29], ComBat++ [35], and CovBat [5] on two tasks: age regression and Alzheimer's disease classification. IRM learns invariant correlations, by regularizing with an optimal naive predictor across all environments (training samples), which allows it to generalize to new test distributions. We implement IRM and ComBat algorithms with the publicly available code and apply the method to the datasets following the best practice. We also show results obtained by training directly on the target data which acts as upper-bound on the performance of harmonization.

4.2   Density estimation

We quantitatively compare the associative capabilities of affine, linear autoregressive spline [7], and quadratic autoregressive spline [10] normalizing flow models by evaluating their total log-likelihood as shown in the Appendix. For both iSTAGING and ADNI datasets, the performance improves consistently with the

Table 1: Age prediction MAE comparison in iSTAGING consortium. All experiments were repeated 5 times in cross-validation fashion, and the average performance is reported with the standard errors in the brackets. TarOnly indicates validation MAEs directly trained on each target sites. The hypothesis that our proposed methods achieve a better accuracy than the baselines can be accepted with p-values between $0.06-0.41$. Age regression task can be interpreted as a sanity check for our method.

| | Study | TarOnly | SrcOnly | IRM | ComBat | | | | Flow-based SCM (ours) | | |
					Linear	GAM	ComBat++	CovBat	Affine	L-Spline	Q-Spline
Source	BLSA-3T	-	11.74 (0.35)	11.76 (0.35)	11.72 (0.62)	11.74 (0.61)	11.73 (0.62)	11.74 (0.62)	11.74 (0.61)	11.74 (0.61)	11.65 (0.62)
Target	BLSA-1.5T	6.77 (0.82)	7.21 (0.91)	7.16 (0.87)	7.14 (0.99)	7.01 (0.99)	7.00 (1.04)	7.03 (1.08)	7.01 (1.01)	7.00 (1.04)	6.92 (1.09)
Target	UKBB	6.14 (0.16)	7.27 (0.70)	7.18 (0.58)	6.62 (0.46)	6.70 (0.46)	6.71 (0.47)	6.75 (0.49)	6.72 (0.46)	6.75 (0.47)	6.44 (0.28)
Target	SHIP	11.36 (0.31)	17.14 (0.62)	17.05 (0.46)	15.95 (0.61)	16.17 (0.59)	16.21 (0.47)	16.22 (0.65)	16.20 (0.59)	16.25 (0.63)	15.68 (0.80)

model's expressive power. The spline autoregressive flow models (17.22 for linear-spline, and 17.24 for quadratic-spline in log-likelihood) show much better density estimation ability compared to simple affine flow model (1.88 in log-likelihood), while quadratic-spline model shows slightly higher log-likelihood than the linear-spline model in iSTAGING dataset.

After we obtained the trained flow-based SCM, counterfactual inference is performed to harmonize scans in ADNI and iSTAGING datasets. We show the feature (hippocampus volume) distributions of raw data, ComBat [16,29] transformed data, and flow-based SCM generated data respectively from iSTAGING consortium in Fig. 2. We find that the feature distributions are not consistent with different means and variances inter-site in raw data. The ComBat transformed feature distributions show relatively consistent means (all shifted to an average value cross-site) resulting from site location and scale effects removal process in the method. The flow-based SCM generated data are counterfactual queries where the scans are all came from site BLSA-3T. We observe similar feature distributions in SCM compared to the raw data, since the proposed method preserves the unknown confounders (subject-specific information due to biological variability, such as race, gene, and pathology AD/CN) by formulating them as exogenous noises in the SCM.

4.3 Age prediction

We compare the generalization abilities of model trained on raw data, site-removed data generated by ComBat [16,29] and its variants [35,5], and counterfactuals generated by flow-based SCM and IRM [1] model trained on raw data for age prediction task as shown in Table 1. All models are firstly trained on BLSA-3T (source site) and then tested on BLSA-1.5T, UKBB, and SHIP separately. We compare the performance of each algorithm on the regression MAE

Table 2: AD classification accuracy (%) comparison in ADNI dataset. All experiments were repeated 5 times in cross-validation fashion, and the average performance is reported with the standard errors in the brackets. TarOnly indicates validation classification accuracies directly trained on each target sites. The hypothesis that our proposed method (Q-Spline) achieves a better accuracy than baselines can be accepted with p-values less than 10^{-5}.

| | Study | TarOnly | SrcOnly | IRM | ComBat | | | | Flow-based SCM (ours) | | |
					Linear	GAM	ComBat++	CovBat	Affine	L-Spline	Q-Spline
Source	ADNI-1	-	76.1 (1.54)	76.2 (2.46)	75.1 (1.37)	75.1 (1.23)	65.1 (6.29)	74.4 (2.29)	76.1 (1.92)	75.3 (1.76)	75.4 (2.45)
Target	ADNI-2	75.8 (3.46)	71.9 (4.88)	73.0 (4.85)	71.4 (4.30)	72.1 (2.83)	56.2 (9.29)	67.4 (5.06)	73.4 (3.52)	72.6 (3.48)	73.7 (4.13)
Source	ADNI-2	-	75.8 (3.46)	76.3 (2.35)	77.5 (2.30)	77.0 (2.74)	67.8 (9.42)	77.9 (2.47)	78.7 (1.32)	78.2 (2.80)	77.5 (1.76)
Target	ADNI-1	76.1 (1.54)	70.4 (8.80)	72.0 (2.16)	71.1 (4.07)	70.1 (5.67)	58.0 (6.28)	69.1 (5.82)	71.4 (2.41)	71.8 (5.76)	73.3 (3.04)

in target site. We find that model (SrcOnly) trained on the source site with raw data couldn't generalize on the target sites. Models trained with site-removed data generated by ComBat generalize much better compared to the one trained on raw data (SrcOnly), whereas IRM models show marginal improvement compared to SrcOnly model. All variants (affine, linear-spline, quadratic-spline) of flow-based SCM show substantial MAE decrements, especially, quadratic-spline SCM outperforms the other methods on all target sites.

4.4   Alzheimer's disease classification

Similar to age prediction, we evaluate model generalizibility when training on the raw data, Combat-harmonized data, and SCM-generated counterfactuals from ADNI dataset for AD classification task. All models are firstly trained on the source sites (ADNI-1 or ADNI-2) and then tested on the target sites (ADNI-2 or ADNI-1) respectively. We compare the performance of each algorithm on the classification accuracy in target site. We also find that there are significant generalization gaps between source and target sites when training with raw data (SrcOnly). ComBat methods show limitations in this task compared to age regression, whereas IRM models have more stable performance. Each variant of flow-based SCM improved the testing accuracy substantially and quadratic-spline SCM models again outperform all other methods.

5   Conclusion

In this paper, we tackle the confounding variations problem from a causal perspective. By explicitly modeling the causal relationship of confounders such as sex, age, and site, and imaging data using our proposed flow-based SCM, we can

harmonize the site-effects by performing counterfactual inference. Our model has demonstrated improved robustness in both regression and classification tasks on a wide range of real-world datasets compared to state-of-the-art algorithms, such as IRM and ComBat. Furthermore, our proposed framework can be enhanced by introducing more confoundings such as race and genetic information. Future directions for this work include causal graph identification and mediation.

Acknowledgements

References

1. Arjovsky, M., Bottou, L., Gulrajani, I., Lopez-Paz, D.: Invariant risk minimization. arXiv preprint arXiv:1907.02893 (2019)
2. Armstrong, N.M., An, Y., Beason-Held, L., Doshi, J., Erus, G., Ferrucci, L., Davatzikos, C., Resnick, S.M.: Predictors of neurodegeneration differ between cognitively normal and subsequently impaired older adults. Neurobiology of aging **75**, 178–186 (2019)
3. Bashyam, V.M., Doshi, J., Erus, G., Srinivasan, D., Abdulkadir, A., Habes, M., Fan, Y., Masters, C.L., Maruff, P., Zhuo, C., et al.: Medical image harmonization using deep learning based canonical mapping: Toward robust and generalizable learning in imaging. arXiv preprint arXiv:2010.05355 (2020)
4. Bingham, E., Chen, J.P., Jankowiak, M., Obermeyer, F., Pradhan, N., Karaletsos, T., Singh, R., Szerlip, P., Horsfall, P., Goodman, N.D.: Pyro: Deep universal probabilistic programming. The Journal of Machine Learning Research **20**(1), 973–978 (2019)
5. Chen, A.A., Beer, J.C., Tustison, N.J., Cook, P.A., Shinohara, R.T., Shou, H.: Removal of scanner effects in covariance improves multivariate pattern analysis in neuroimaging data. bioRxiv p. 858415 (2020)
6. Davatzikos, C.: Machine learning in neuroimaging: Progress and challenges. NeuroImage **197**, 652 (2019)
7. Dolatabadi, H.M., Erfani, S., Leckie, C.: Invertible generative modeling using linear rational splines. arXiv preprint arXiv:2001.05168 (2020)
8. Doshi, J., Erus, G., Ou, Y., Gaonkar, B., Davatzikos, C.: Multi-atlas skull-stripping. Academic radiology **20**(12), 1566–1576 (2013)
9. Doshi, J., Erus, G., Ou, Y., Resnick, S.M., Gur, R.C., Gur, R.E., Satterthwaite, T.D., Furth, S., Davatzikos, C., Initiative, A.N., et al.: Muse: Multi-atlas region segmentation utilizing ensembles of registration algorithms and parameters, and locally optimal atlas selection. Neuroimage **127**, 186–195 (2016)
10. Durkan, C., Bekasov, A., Murray, I., Papamakarios, G.: Neural spline flows. In: Advances in Neural Information Processing Systems. pp. 7511–7522 (2019)
11. Esteva, A., Kuprel, B., Novoa, R.A., Ko, J., Swetter, S.M., Blau, H.M., Thrun, S.: Dermatologist-level classification of skin cancer with deep neural networks. nature **542**(7639), 115–118 (2017)

12. Goodfellow, I., Pouget-Abadie, J., Mirza, M., Xu, B., Warde-Farley, D., Ozair, S., Courville, A., Bengio, Y.: Generative adversarial nets. In: Advances in neural information processing systems. pp. 2672–2680 (2014)
13. Habes, M., Pomponio, R., Shou, H., Doshi, J., Mamourian, E., Erus, G., Nasrallah, I., Launer, L.J., Rashid, T., Bilgel, M., et al.: The brain chart of aging: Machine-learning analytics reveals links between brain aging, white matter disease, amyloid burden, and cognition in the istaging consortium of 10,216 harmonized mr scans. Alzheimer's & Dementia **17**(1), 89–102 (2021)
14. Hegenscheid, K., Kühn, J.P., Völzke, H., Biffar, R., Hosten, N., Puls, R.: Whole-body magnetic resonance imaging of healthy volunteers: pilot study results from the population-based ship study. In: RöFo-Fortschritte auf dem Gebiet der Röntgenstrahlen und der bildgebenden Verfahren. vol. 181, pp. 748–759. © Georg Thieme Verlag KG Stuttgart· New York (2009)
15. Jack Jr, C.R., Bernstein, M.A., Fox, N.C., Thompson, P., Alexander, G., Harvey, D., Borowski, B., Britson, P.J., L. Whitwell, J., Ward, C., et al.: The alzheimer's disease neuroimaging initiative (adni): Mri methods. Journal of Magnetic Resonance Imaging: An Official Journal of the International Society for Magnetic Resonance in Medicine **27**(4), 685–691 (2008)
16. Johnson, W.E., Li, C., Rabinovic, A.: Adjusting batch effects in microarray expression data using empirical bayes methods. Biostatistics **8**(1), 118–127 (2007)
17. Kingma, D.P., Ba, J.: Adam: A method for stochastic optimization. arXiv preprint arXiv:1412.6980 (2014)
18. Kingma, D.P., Welling, M.: Auto-encoding variational bayes. arXiv preprint arXiv:1312.6114 (2013)
19. Menze, B.H., Jakab, A., Bauer, S., Kalpathy-Cramer, J., Farahani, K., Kirby, J., Burren, Y., Porz, N., Slotboom, J., Wiest, R., et al.: The multimodal brain tumor image segmentation benchmark (brats). IEEE transactions on medical imaging **34**(10), 1993–2024 (2014)
20. Morris, C.N.: Parametric empirical bayes inference: theory and applications. Journal of the American statistical Association **78**(381), 47–55 (1983)
21. Moyer, D., Gao, S., Brekelmans, R., Galstyan, A., Ver Steeg, G.: Invariant representations without adversarial training. Advances in Neural Information Processing Systems **31**, 9084–9093 (2018)
22. Moyer, D., Ver Steeg, G., Tax, C.M., Thompson, P.M.: Scanner invariant representations for diffusion mri harmonization. Magnetic Resonance in Medicine (2020)
23. Papamakarios, G., Nalisnick, E., Rezende, D.J., Mohamed, S., Lakshminarayanan, B.: Normalizing flows for probabilistic modeling and inference. arXiv preprint arXiv:1912.02762 (2019)
24. Papamakarios, G., Pavlakou, T., Murray, I.: Masked autoregressive flow for density estimation. In: Advances in Neural Information Processing Systems. pp. 2338–2347 (2017)
25. Paszke, A., Gross, S., Massa, F., Lerer, A., Bradbury, J., Chanan, G., Killeen, T., Lin, Z., Gimelshein, N., Antiga, L., et al.: Pytorch: An imperative style, high-performance deep learning library. In: Advances in neural information processing systems. pp. 8026–8037 (2019)
26. Pearl, J.: Causality: Models, reasoning, and inference. Cambridge University Press, 2nd edition (2009)
27. Pearl, J., et al.: Causal inference in statistics: An overview. Statistics surveys **3**, 96–146 (2009)
28. Peters, J., Janzing, D., Schölkopf, B.: Elements of causal inference. The MIT Press (2017)

29. Pomponio, R., Erus, G., Habes, M., Doshi, J., Srinivasan, D., Mamourian, E., Bashyam, V., Nasrallah, I.M., Satterthwaite, T.D., Fan, Y., et al.: Harmonization of large mri datasets for the analysis of brain imaging patterns throughout the lifespan. NeuroImage **208**, 116450 (2020)
30. Resnick, S.M., Pham, D.L., Kraut, M.A., Zonderman, A.B., Davatzikos, C.: Longitudinal magnetic resonance imaging studies of older adults: a shrinking brain. Journal of Neuroscience **23**(8), 3295–3301 (2003)
31. Robinson, R., Dou, Q., de Castro, D.C., Kamnitsas, K., de Groot, M., Summers, R.M., Rueckert, D., Glocker, B.: Image-level harmonization of multi-site data using image-and-spatial transformer networks. In: International Conference on Medical Image Computing and Computer-Assisted Intervention. pp. 710–719. Springer (2020)
32. Schölkopf, B.: Causality for machine learning. arXiv preprint arXiv:1911.10500 (2019)
33. Sudlow, C., Gallacher, J., Allen, N., Beral, V., Burton, P., Danesh, J., Downey, P., Elliott, P., Green, J., Landray, M., et al.: Uk biobank: an open access resource for identifying the causes of a wide range of complex diseases of middle and old age. Plos med **12**(3), e1001779 (2015)
34. Tustison, N.J., Avants, B.B., Cook, P.A., Zheng, Y., Egan, A., Yushkevich, P.A., Gee, J.C.: N4itk: improved n3 bias correction. IEEE transactions on medical imaging **29**(6), 1310–1320 (2010)
35. Wachinger, C., Rieckmann, A., Pölsterl, S., Initiative, A.D.N., et al.: Detect and correct bias in multi-site neuroimaging datasets. Medical Image Analysis **67**, 101879 (2021)
36. Zhu, J.Y., Park, T., Isola, P., Efros, A.A.: Unpaired image-to-image translation using cycle-consistent adversarial networks. In: Proceedings of the IEEE international conference on computer vision. pp. 2223–2232 (2017)

Appendix

Table 3: Summary of participant demographics in iSTAGING consortium. Age is described in format: mean ± std [min, max]. F and M in gender represent female and male separately. Field indicates the magnetic strength of the MRI scanners.

Study	Subject	Age	Gender (F/M)	Field
BLSA-1.5T	157	69.1 ± 8.5 [48.0, 85.0]	66 / 91	1.5T
BLSA-3T	960	65.0 ± 14.7 [22.0, 93.0]	525 / 435	3T
UKBB	2202	62.8 ± 7.3 [45.0, 79.0]	1189 / 1013	3T
SHIP	2739	52.6 ± 13.7 [21.2, 90.4]	1491 / 1248	1.5T

Table 4: Summary of participant demographics in ADNI dataset. Age is described in format: mean ± std [min, max]. F and M in gender represent female and male separately. Field indicates the magnetic strength of the MRI scanners.

Study	Subject	CN	AD	Age	Gender (F/M)	Field
ADNI-1	422	229	193	75.5 ± 6.2 [55.0, 90.9]	201 / 221	1.5T
ADNI-2/GO	441	294	147	73.4 ± 6.8 [55.4, 90.3]	221 / 220	3T

Table 5: Multi-layer perceptron (MLP) network implementation details. The network is used for age regression and AD classification tasks. The output size k of the final layer is depends on the task.

Layer	Input Size	LeakyReLU α	Output Size
Linear + LeakyReLU	145	0.1	72
Linear + LeakyReLU	72	0.1	36
Linear	36	-	k

Table 6: Flow-based SCM implementation details. We directly learn the binary probability of sex s and categorical probability of site t. p_θ^S and p_θ^T are the learnable mass functions of the categorical distribution for variables sex s and site t, and K is the number of site t. The modules indicated with θ are parameterized using neural networks. We constrain age a variable with lower bound (exponential transform) and rescale it with fixed affine transform for normalization. Spline$_\theta$ transformation refers to the linear neural spline flows [7]. The ConditionalTransform$_\theta(\cdot)$ can be conditional affine or conditional spline transform, which reparameterizes the noise distribution into another Gaussian distribution. We use linear [7] and quadratic [10] autoregressive neural spline flows for the conditional spline transform, which are more expressive compared to the affine flows. The transformation parameters of the ConditionalTransform$_\theta(\cdot)$ are predicted by a context neural network taking $\cdot$ as input. The context networks are implemented as fully-connected networks for affine and spline flows.

| Observations	Exogenous noise
$s := \epsilon_S$	$\epsilon_S \sim \mathrm{Ber}(p_\theta^S)$
$a := f_A(\epsilon_A) = (\mathrm{Spline}_\theta \circ \mathrm{Affine} \circ \mathrm{Exp})(\epsilon_A)$	$\epsilon_A \sim \mathcal{N}(0,1)$
$t := \epsilon_T$	$\epsilon_T \sim \mathrm{Cat}(K, p_\theta^T)$
$x := f_X(\epsilon_X; s, a, t) = (\mathrm{ConditionalTransform}_\theta([s,a,t]))(\epsilon_X)$	$\epsilon_X \sim \mathcal{N}(0,1)$

Table 7: Comparison of associative abilities of different type of flows on iSTAGING consortium and ADNI dataset. We observe that spline flows achieved higher log-likelihood compared to that of affine flow for both datasets. This indicates that a flow with higher expressive power helps for density estimation.

Study	Model	Log-likelihood
iSTAGING	Affine	1.8817
	Linear Spline	17.2204
	Quadratic Spline	17.2397
ADNI	Affine	1.8963
	Linear Spline	15.2715
	Quadratic Spline	15.2055
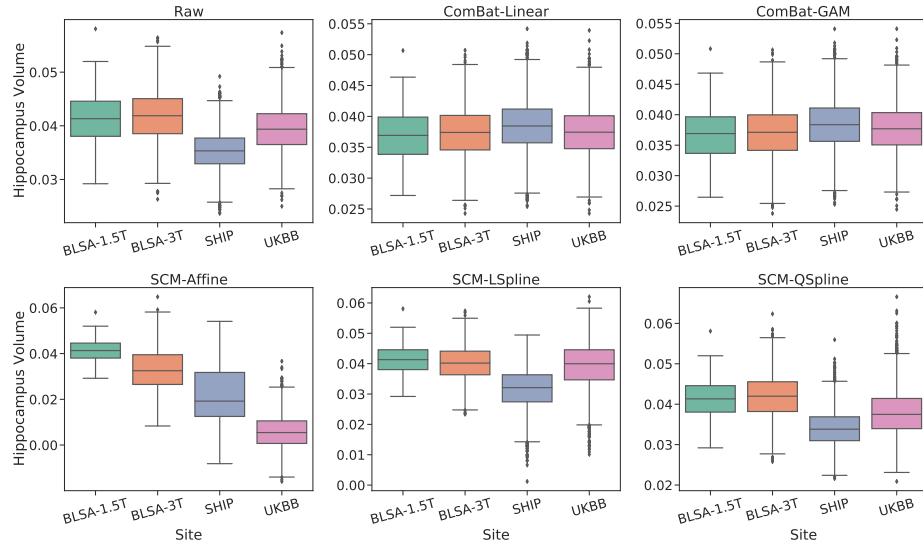
(a) Hippocampus (Right)
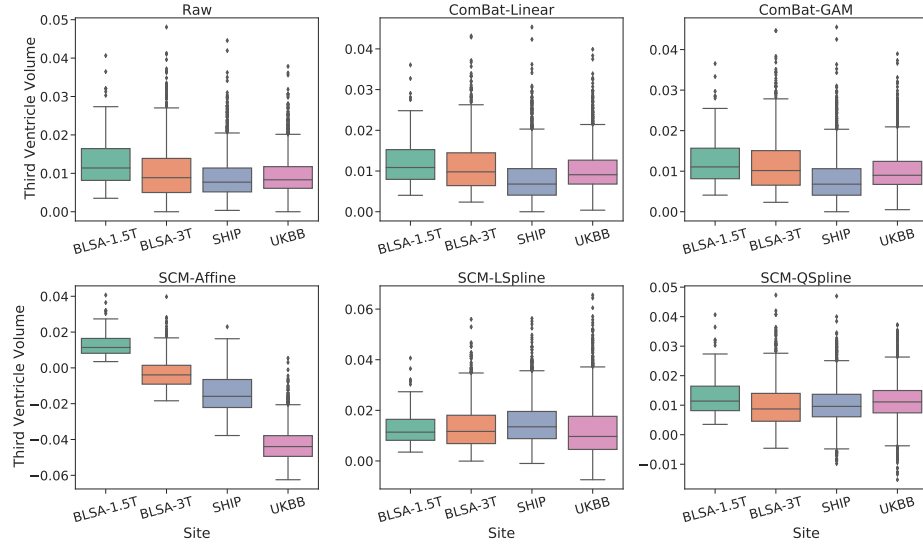
(b) Third Ventricle (Right)

Fig. 3: Comparison of normalized feature distributions cross-site in iSTAGING consortium before and after apply the ComBat methods (ComBat-Linear and ComBat-GAM) and the proposed methods (SCM-Affine, SCM-LSpline, and SCM-QSpline). The distributions of the features harmonized by ComBat methods are aligned cross-site, whereas those harmonized by our proposed method (Q-Spline) are unchanged compared to the raw features. We preserve the unknown cofounders (subject-specific information due to biological variability, such as race, gene, and pathology AD/CN) instead of removing them as site-effects, which is beneficial for downstream analysis, such as AD diagnosis.
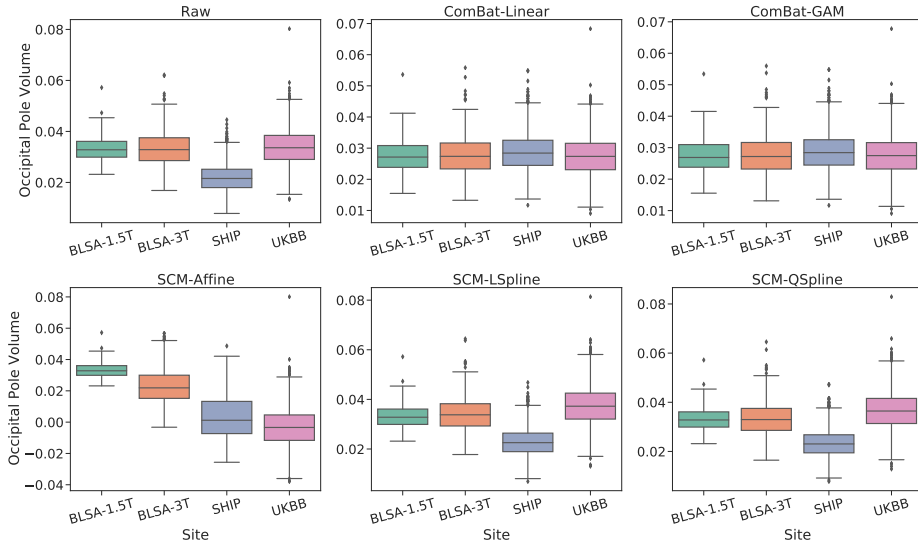
(a) Occipital Pole
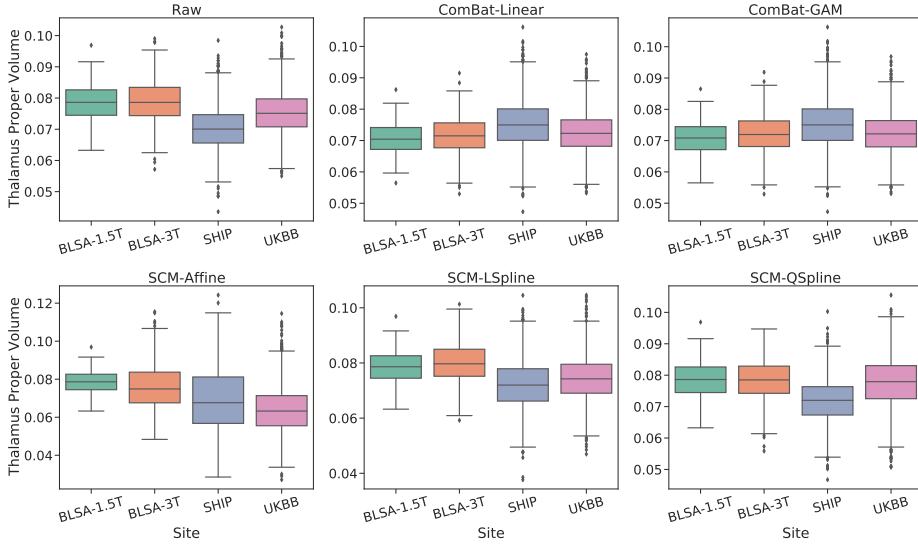
(b) Thalamus Proper (Right)

Fig. 4: Continued comparison of normalized feature distributions cross-site in iSTAGING consortium before and after apply the ComBat methods (ComBat-Linear and ComBat-GAM) and the proposed methods (SCM-Affine, SCM-LSpline, and SCM-QSpline). The distributions of the features harmonized by ComBat methods are aligned cross-site, whereas those harmonized by our proposed method (Q-Spline) are unchanged compared to the raw features. We preserve the unknown cofounders (subject-specific information due to biological variability, such as race, gene, and pathology AD/CN) instead of removing them as site-effects, which is beneficial for downstream analysis, such as AD diagnosis.